NASA TECHNICAL NOTE

NASA TN D-3618

NASA TN D-3618

AN INVESTIGATION OF SPRAY VELOCITY RESULTING FROM HIGH-VELOCITY PENETRATION OF THIN PLATES BY DISKS

by John D. Di Battista

Langley Research Center
Langley Station, Hampton, Va.

NATIONAL AERONAUTICS AND SPACE ADMINISTRATION • WASHINGTON, D. C. • SEPTEMBER 1966

AN INVESTIGATION OF SPRAY VELOCITY RESULTING FROM HIGH-VELOCITY PENETRATION OF THIN PLATES BY DISKS

By John D. Di Battista

Langley Research Center
Langley Station, Hampton, Va.

NATIONAL AERONAUTICS AND SPACE ADMINISTRATION

For sale by the Clearinghouse for Federal Scientific and Technical Information
Springfield, Virginia 22151 – Price $2.00

AN INVESTIGATION OF SPRAY VELOCITY RESULTING FROM HIGH-VELOCITY PENETRATION OF THIN PLATES BY DISKS*

By John D. Di Battista
Langley Research Center

SUMMARY

An analysis based on one-dimensional shock-wave theory is presented to study the maximum velocity of the spray emanating from the rear surface of a thin meteoroid bumper. A set of experiments was designed to evaluate the analytical results. The targets used were 0.0025-cm-thick 1100 aluminum foil and 0.041-cm-thick 1100 H14 aluminum plate. The projectiles used were made of tungsten and were disk shaped, 0.56 cm in diameter, and either 0.076 cm or 0.038 cm in thickness. The target and projectile dimensions used in the experiments insured that the one-dimensional assumptions used in the theory were valid. In addition, using a very dense tungsten projectile to impact the aluminum targets produced aluminum spray velocities well in excess of the tungsten projectile velocity. With this technique, the projectile and target materials were clearly differentiable in the spray. The experiments were conducted in the impact velocity range of 0.089 to 0.295 cm/μsec.

The ratio of maximum target-material spray velocity to projectile impact velocity is defined and is plotted against projectile impact velocity. The ratio predicted by using the theory agrees well with the experimental results in the range of impact velocities investigated. Representative series of photographs are presented and analyzed for the experiments conducted in both thicknesses of aluminum targets.

INTRODUCTION

Protection against the effects of high velocity meteoroids may be accomplished by utilizing a meteoroid bumper. The meteoroid bumper consists of a thin sheet of material spaced a distance in front of a spacecraft main wall. The function of the bumper is to

*The information presented herein was offered as a thesis in partial fulfillment of the requirements for the degree of Master of Science in Engineering Mechanics, Virginia Polytechnic Institute, Blacksburg, Virginia, June 1966.

break up an impacting meteoroid and produce a diverging spray of smaller particles less damaging than the original meteoroid to the main wall.

The analysis of the impact of a bumper protected spacecraft can be separated into two parts: one dealing with the penetration of the bumper thus establishing the particle sizes and velocities of the spray, and the second dealing with the damage inflicted on the main wall by the impact of this debris. The analysis and experimental data reported herein deal only with the former and, in particular, establish the maximum velocity of spray particles which may strike the main wall.

An experimental technique has been employed which produced a one-dimensional interaction between a thin bumper and an impacting projectile so that the results may be correlated with a one-dimensional analysis of the interaction. A disk-shaped projectile was allowed to impact only on its face with similar thickness targets. The projectile and target materials were chosen as tungsten and aluminum, respectively. The use of a projectile material much denser than the target material caused the maximum spray velocity of the aluminum target material to be much greater than the projectile impact velocity. A ratio of the maximum aluminum spray velocity to the projectile impact velocity was defined and compared with the predicted ratio for the range of impact velocities tested.

SYMBOLS

C'	empirical constant, cm/μsec
C''	empirical constant, dimensionless
P	pressure
U	velocity
ρ	density

Subscripts:

a	rarefaction wave
c	compressed material after shock-wave passage
f	target rear surface

o	uncompressed material before shock-wave passage
p	projectile
r	expanded material after rarefaction-wave passage
s	shock wave

APPARATUS AND TEST TECHNIQUE

Projectiles and Targets

The projectiles were disks 0.56 cm in diameter and either 0.076 cm or 0.038 cm in thickness. They were cut from tungsten plate by using an electrical discharge machining process. The density of the tungsten was 19.26 gm/cm^3.

The tungsten disk projectiles were mounted on nylon sabots of length-to-diameter ratios of either 1 or 1/2. These sabots were sufficient to prevent shattering of the projectile during launch. Figure 1 shows the mounting of a 0.076-cm-thick tungsten disk on a sabot of length-to-diameter ratio of 1 and a 0.038-cm-thick tungsten disk on a sabot of length-to-diameter ratio of 1/2.

The targets were 1100 aluminum foil 0.0025 cm thick and 1100 H14 aluminum plate 0.041 cm thick.

Test Setup and Operation

The complete test setup has been pictured schematically in figure 2. The chambers through which the projectile travels were evacuated to a pressure between 130 and 270 N/m^2. This vacuum eliminated air drag on the projectile and possible air interference with the experiment. The mounted projectiles were loaded into one of two accelerators used. A modified 22-caliber Swift rifle was used to accelerate projectiles in the velocity range of 0.089 cm/μsec to 0.219 cm/μsec and a shock-compressed helium gas gun was used to accelerate projectiles from 0.219 cm/μsec to 0.295 cm/μsec. For a description and photograph of each of these accelerators, see reference 1.

A projectile detection system was located beyond two large blast chambers. The projectile detection system was composed of two reflected-light stations placed 60.9 cm apart. An image-converter photographing system in each station was placed in a vertical view perpendicular to the projectile line of flight. When the projectile appeared at the first station, it passed through a light screen and reflected some of the light into a receiving photomultiplier which then sent a signal to start a time-interval meter. The

same photomultiplier also sent a signal to the image-converter photographing system to take a picture of the projectile. At the second reflected-light station, a similar procedure was repeated with the time-interval meter being stopped. This system gives the information necessary to determine the projectile velocity with an accuracy estimated to be better than ±3 percent. Figure 3 shows two photographs of the tungsten disk taken at the start and stop stations of the system. A time-delay computer then used the time recorded by the projectile detection system to synchronize a 60 μsec duration xenon flash tube with the arrival of the projectile at the target position 167.6 cm behind the last reflected-light station. The thin target was placed with its flat surface perpendicular to the projectile line of flight. A high-speed framing camera was placed in a horizontal view perpendicular to the projectile line of flight and in line with the target edge and xenon flash tube. The xenon flash tube was focused by a Fresnel lens. During a firing the high-speed framing camera was operated at approximately 1 000 000 frames per second with the shutter open in a darkened room. With the arrival of the projectile at the target position the xenon tube flashes allowing the high-speed camera to record the motions of the projectile and spray. About 20 useful frames were obtained for each firing. The velocities of the projectile and maximum target-material spray and the attitude of the projectile from a horizontal view may be determined. Also, the shape of the spray cloud and relative amount of fragmentation of material in the leading part of the spray cloud may be determined from the high-speed framing camera data.

The average percent difference between the two methods of measuring the projectile velocity was 3.18 percent (based on the projectile detection system velocity).

PRESENTATION AND DISCUSSION OF RESULTS

Analytical Development

The one-dimensional shock-wave theory in solids may be used to study the collision of a projectile and thin target. The theory is used to construct a model that predicts the ratio of the maximum target-material spray velocity and projectile impact velocity. The following method was employed to calculate the ratio. First, the free rear surface velocity U_f of a plate subjected to the passage of a strong shock wave and the subsequent reflection of this shock wave as an isentropic expansion wave from the rear surface of the target is determined. The velocity U_f is composed of U_c, a velocity component due to the passage of a strong shock wave traveling at a velocity U_s, and U_r, a velocity component due to the isentropic expansion wave traveling at $U_a - U_c$ shown in figures 4(a) and 4(b). Combining U_c and U_r yields in laboratory coordinates

$$U_f = U_c + U_r \tag{1}$$

The velocity component U_r due to the isentropic expansion of the compressed material at the target rear surface has been the subject of an extensive investigation in aluminum in references 2 and 3. It has been shown in reference 3 that the ratio of U_r/U_c for the region of interest in this investigation (shock pressures between 100 and 500 kilobars) varied from 1.003 to 1.03. Therefore, the ratio of U_r/U_c is assumed to be unity. Then,

$$U_r = U_c \tag{2}$$

Substituting into equation (1) gives

$$U_f = 2U_c \tag{3}$$

Thus, the free rear-surface velocity U_f of a thin target is taken to be twice the velocity component U_c due to the passage of a strong shock wave.

For a shock pressure the velocity component U_c and, therefore, U_f is calculated by using the following two equations. Equation (4) is the experimentally obtained linear relation for commercial aluminum as given in reference 4:

$$U_s = C' + C''U_c \tag{4}$$

where U_s is the shock wave velocity and C' and C'' are constants. Equation (5) is the result of combining the mass and momentum equations for one of the Rankine-Hugoniot jump conditions across a shock:

$$P_c - P_o = \rho_o U_s U_c \tag{5}$$

Here, the newly introduced quantities are P_c, the pressure in the compressed material after passage of the shock wave; P_o, the atmospheric pressure which in relation to P_c is approximately zero; and ρ_o, the original density of the material at P_o. By using equation (4) to eliminate U_s in equation (5), by picking a specific shock pressure, and by arranging the resulting equation the corresponding value of U_c may be calculated from

$$U_c = \frac{-C' + \sqrt{(C')^2 + 4C''\frac{P_c}{\rho_o}}}{2C''} \tag{6}$$

The value of U_f may then be calculated from equation (3).

The impact velocity U_p, necessary to produce a certain value of P_c and associated value of U_f in the target material, is then calculated. Across the interface between the projectile and target material, U_c and P_c for both compressed materials are the same. Figure 5 shows a graphical determination of the projectile impact velocity using the matching Hugoniot technique. The curves of U_c as a function of P_c for the

aluminum target material and tungsten projectile material (ref. 5) are plotted in figure 5. The intersection of the two curves expresses the equality of the velocity U_c for the compressed target and projectile materials and the pressure P_c for the compressed target and projectile materials during impact. The impact velocity of the projectile U_p necessary to produce a specific U_c and P_c is given at the intersection of the reflected projectile Hugoniot with the abscissa. Thus, with this procedure, the ratio of U_f/U_p and its dependency on U_p may be determined.

Design of Experiment

In order that the one-dimensional analysis be valid during the impact process, the dimensions of the projectile and targets must be carefully selected. The dimensions of the projectile are governed by the diameter of the gun barrel (0.56 cm for this investigation) and the requirement that the gun accelerate the thickest possible projectile without critically inhibiting its velocity performance. The desired target thickness depends directly on the physical dimensions of the projectile in that the shock wave traveling in the target material could be affected by rarefaction waves emanating from the rear and side of the projectile.

On the assumption that the impact between the face of the disk-shaped projectile and target was flat, calculations showed that rarefaction waves emanating from the rear of the projectiles never affected the shock wave in the aluminum targets. For the rarefaction waves emanating from the sides of the projectile, the calculations showed that the amount of the shock front affected for the 0.0025-cm-thick targets was less than 2 percent of the projectile radius and for the 0.041-cm-thick targets was less than 20 percent of the projectile radius for all cases covered in the experiment.

The selection of the aluminum target and tungsten projectile material combination was based on several considerations. The Hugoniot curves for both materials were obtainable from references 4 and 5. Also, the one-dimensional shock-wave theory indicates that the maximum aluminum spray velocity is greater than the tungsten disk impact velocity. This difference in velocity made photographing the target spray very convenient and allowed differentiation of target spray and projectile spray in the photographic data.

Comparison of Analytical and Experimental Results

The analytical ratio of U_f/U_p as a function of U_p is plotted in figures 6 and 7 as a solid line. The experimental ratio of maximum aluminum spray velocity and tungsten projectile impact velocity has been tabulated in table 1 for the corresponding experimental impact velocity. The points were plotted as circles on figures 6 and 7. The experimental points may be seen to agree well with the predicted values for the range of velocities tested.

Representative series of photographs of the penetration experimental data into the 0.0025-cm-thick targets are presented in figures 8 to 12. These figures are placed in order of increasing impact velocity. The impact velocity range for these shots covered from 0.113 cm/μsec to 0.295 cm/μsec.

Figure 8 shows a very fine mist at 2.26μsec after impact. By 9.04 μsec after impact, this mist has become dispersed, being invisible to the camera, and a discrete particle of aluminum material is seen leading the spray. The velocity of this aluminum particle was taken to be the maximum aluminum spray velocity. Also, the tungsten disk may be seen to be intact at the back of the spray cloud.

In figure 9 the disk may be seen to be slightly but distinctly separated from the nylon sabot. These photographs show an air shock wave preceding the projectile and again preceding the spray. The effect of this amount of air on the maximum aluminum spray velocity is negligible. The ratio of the maximum target-material spray velocity to the projectile impact velocity is 1.59, which is similar to that of other tests where no air shock waves could be seen. It may be noted that the leading portion of the spray cloud appears to be composed now of a number of particles.

The cloud of target spray material in figure 10 is more finely fragmented than shown in the two previous figures. A fine mist of particles and several tiny jets precede the dense cloud of particles. The fine mist, however, was not used in determining the spray velocity. The maximum velocity of the spray cloud was taken as the boundary of the very dense region.

In figure 11 is illustrated experimental data which are difficult to interpret in terms of maximum spray velocity. Two long dagger-shaped sprays may be seen to have a tip velocity of 2.42 times the impact velocity of 0.243 cm/μsec. Their presence could be explained by possible surface irregularities on the target or projectile or a possible contaminant. However, because nothing irregular prior to impact could be found, the result was included in the plot for comparison with the predicted values.

The highest velocity impact is shown in figure 12. This impact velocity was achieved when the lighter 0.038-cm-thick tungsten disk was used. This projectile acts in the same manner as the thicker projectile in insuring that the one-dimensional shock conditions are established and maintained for a sufficient length of time. The aluminum target material is very finely fragmented and is followed by the slightly fragmented tungsten disk.

The 0.0025-cm-thick aluminum targets provided a test of the ability of the framing camera and xenon-tube backlighting system to photograph the leading edge of the aluminum sprays produced from extremely thin targets. The sensitivity has been demonstrated by figures 8 to 12 where the aluminum sprays have been clearly visible to the camera over

the experimental impact-velocity range tested. In fact, the test setup appears to be sufficiently sensitive to record the spray from targets thinner than 0.0025 cm.

Figures 13 to 18 arranged in order of increasing projectile velocity illustrate the impacts into the 0.041-cm-thick targets in the velocity range from 0.089 to 0.291 cm/μsec.

A large particle of the aluminum target at the front of the spray cloud may be seen quite clearly in figure 13 at 8.24 μsec and 17.53 μsec after impact. This particle exhibited rotation as it traversed the field of view.

In figure 14 a discrete particle of aluminum leads the spray 12.84 μsec after impact. It can be noted that the 0.0025-cm-thick targets at this impact velocity did not fragment the tungsten projectile. However, in penetrating the thicker 0.041-cm targets, the projectile was fractured and appears as a trapezoid with base forward in the center of the spray cloud at 12.84 μsec.

The leading spray in figure 15 is composed of many small fragments. The fractured tungsten disk may again be seen in the center of the spray cloud.

Figure 16 has been included in the series to illustrate a very rapidly moving jet formed at the top of the leading portion of the spray cloud. The jet may be seen at 2.30 μsec and 4.60 μsec after impact of the 0.076-cm-thick projectile. However, at 9.20 μsec after impact, the jet was too dispersed to be seen by the camera. The maximum target-material velocity was taken from the velocity of the flat leading portion of the spray cloud. The shattered projectile is again further back in the spray cloud.

In figure 17 the spray and the projectile are again shown in a fragmented condition.

The highest impact velocity achieved into the 0.041-cm-thick targets is shown in figure 18. The 0.038-cm-thick projectile was used. This change in projectile thickness does not affect the maximum target-material spray velocity. The frames 7.91 μsec and 9.04 μsec after impact show twin jets preceding the main body of spray. The maximum target-material spray velocity was taken from the leading-edge velocity of the elliptically shaped cloud.

The impacts into the very thin (0.0025-cm-thick) targets produced spray clouds which showed very little lateral expansion of the target-material spray, whereas the impacts into the thicker (0.041-cm) targets produced the familiar elliptically shaped cloud profiles. The change in spray cloud profile was produced by the increased role played by lateral rarefaction waves in the thicker target. Another point to be noted is the requirement for a flat impact between the target and projectile faces to generate experimentally a one-dimensional flow in the target. The conditions in figure 19 were almost identical with those of figure 18 except for the projectile attitude. The resulting ratio for the maximum aluminum target-material velocity and projectile impact velocity was equal to 1.00 for figure 19, as compared with the 1.62 ratio for figure 18.

CONCLUDING REMARKS

Very dense disk-shaped projectiles unskewed and intact were accelerated to high velocities. This allowed the experimental results of the interaction of a thin bumper target and impacting projectile to be correlated with the one-dimensional shock-wave theory. Good agreement between the experimental and analytical results was shown for the ratio of the maximum target-material spray velocity to the projectile impact velocity in the impact velocity range tested. The agreement between the predicted and experimental results justified the interaction model used.

As the projectile impact velocity increased, the photographic records showed an increase in fragmentation of the target material and also an increase in projectile fragmentation as target thickness increased.

Langley Research Center,
National Aeronautics and Space Administration,
Langley Station, Hampton, Va., May 19, 1966.

REFERENCES

1. Collins, Rufus D., Jr.; and Kinard, William H.: The Dependency of Penetration on the Momentum Per Unit Area of the Impacting Projectile and the Resistance of Materials to Penetration. NASA TN D-238, 1960.

2. Walsh, John M.; and Christian, Russell H.: Equation of State of Metals From Shock Wave Measurements. Phys. Rev., second ser., vol. 97, no. 6, Mar. 15, 1955, pp. 1544-1556.

3. Walsh, John M.; Rice, Melvin H.; McQueen, Robert G.; and Yarger, Frederick L.: Shock-Wave Compressions of Twenty-Seven Metals. Equations of State of Metals. Phys. Rev., second ser., vol. 108, no. 2, Oct. 15, 1957, pp. 196-216.

4. Duvall, G. E.; and Fowles, G. R.: Shock Waves. High Pressure Physics and Chemistry, Vol. 2, R. S. Bradley, ed., Academic Press, 1963, pp. 209-291.

5. McQueen, R. G.; and Marsh, S. P.: Equation of State for Nineteen Metallic Elements From Shock-Wave Measurements to Two Megabars. J. Appl. Phys., vol. 31, no. 7, July 1960, pp. 1253-1269.

TABLE 1.- TABULATED DATA

Shot	Target properties		Projectile properties				Projectile velocity, cm/μsec	Ratio of maximum spray velocity to projectile velocity
	Material	Thickness, cm	Material	Shape	Diameter, cm	Thickness, cm		
1	1100 aluminum	0.0025	Tungsten	Disk	0.56	0.076	0.113	1.52
2	1100 aluminum	.0025	Tungsten	Disk	.56	.076	.135	1.55
3	1100 aluminum	.0025	Tungsten	Disk	.56	.076	.179	1.59
4	1100 aluminum	.0025	Tungsten	Disk	.56	.076	.219	1.74
5	1100 aluminum	.0025	Tungsten	Disk	.56	.076	.243	2.42
6	1100 aluminum	.0025	Tungsten	Disk	.56	.038	.295	1.69
7	1100 H14 aluminum	.041	Tungsten	Disk	.56	.076	.089	1.48
8	1100 H14 aluminum	.041	Tungsten	Disk	.56	.076	.137	1.68
9	1100 H14 aluminum	.041	Tungsten	Disk	.56	.076	.143	1.58
10	1100 H14 aluminum	.041	Tungsten	Disk	.56	.076	.162	1.71
11	1100 H14 aluminum	.041	Tungsten	Disk	.56	.076	.209	1.59
12	1100 H14 aluminum	.041	Tungsten	Disk	.56	.076	.212	1.62
13	1100 H14 aluminum	.041	Tungsten	Disk	.56	.076	.250	1.59
14	1100 H14 aluminum	.041	Tungsten	Disk	.56	.076	.270	1.65
15	1100 H14 aluminum	.041	Tungsten	Disk	.56	.076	.273	1.76
16	1100 H14 aluminum	.041	Tungsten	Disk	.56	.038	.291	1.62
17	1100 H14 aluminum	.041	Tungsten	Disk	.56	.038	.294	1.00

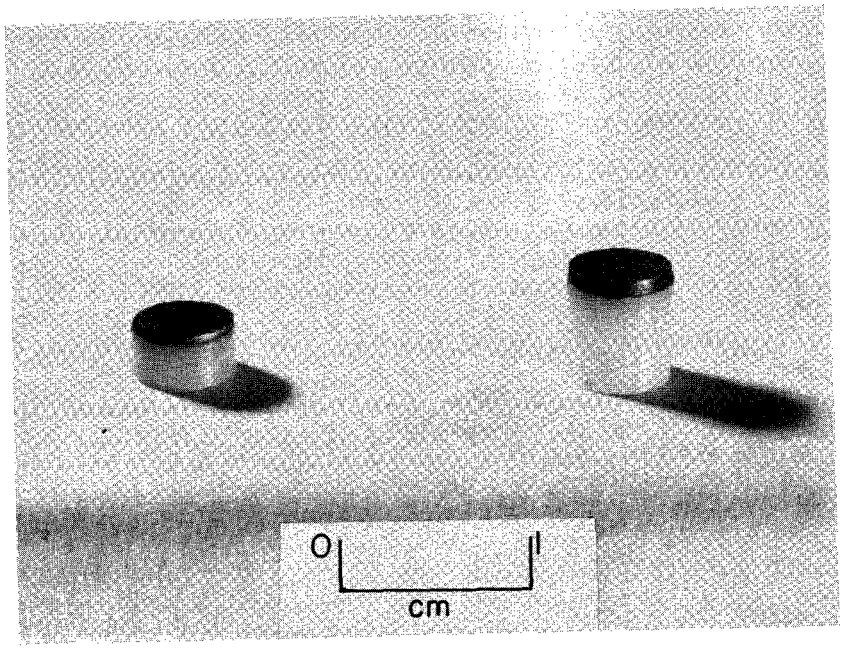

Left projectile

Tungsten disk

.56 cm in diameter

.038 cm in thickness mounted on nylon sabot

.56 cm in diameter

.28 cm in thickness

Right projectile

Tungsten disk

.56 cm in diameter

.076 cm in thickness mounted on nylon sabot

.56 cm in diameter

.56 cm in thickness

Figure 1.- Projectiles mounted for firing. L-66-4417

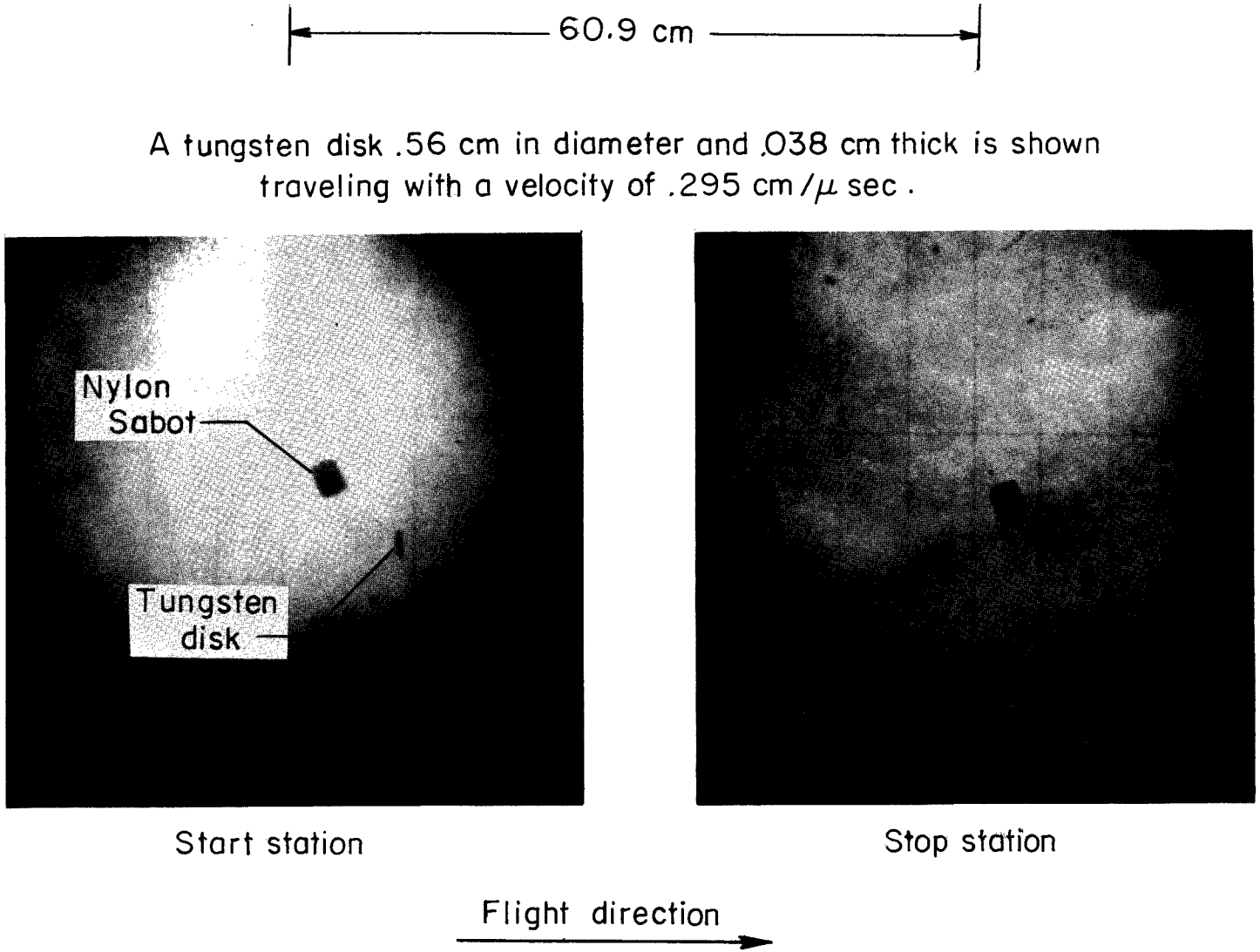

Figure 2.- Schematic of experimental setup.

L-66-4418

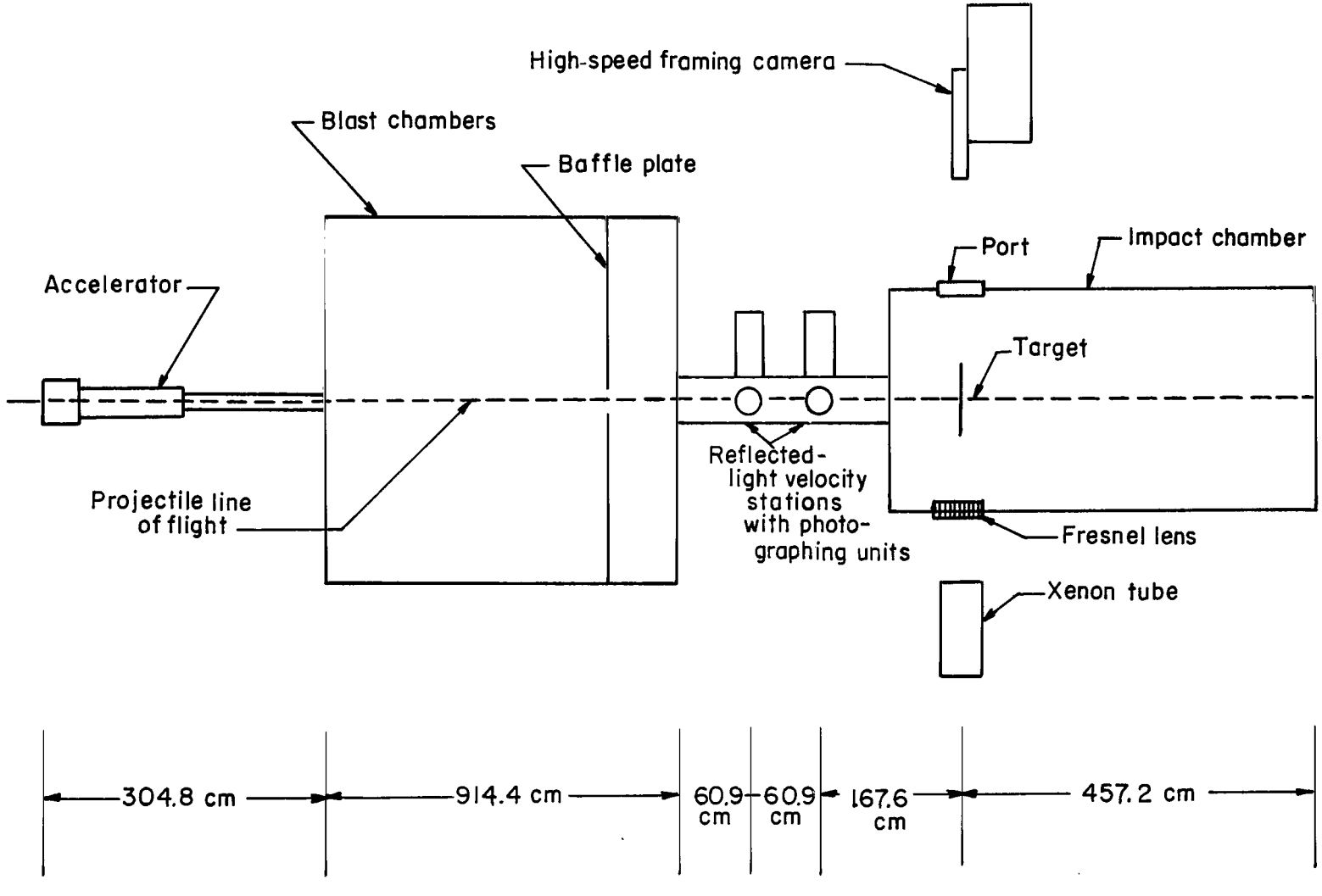

Figure 3.- Projectile photographs taken at the two detection stations.

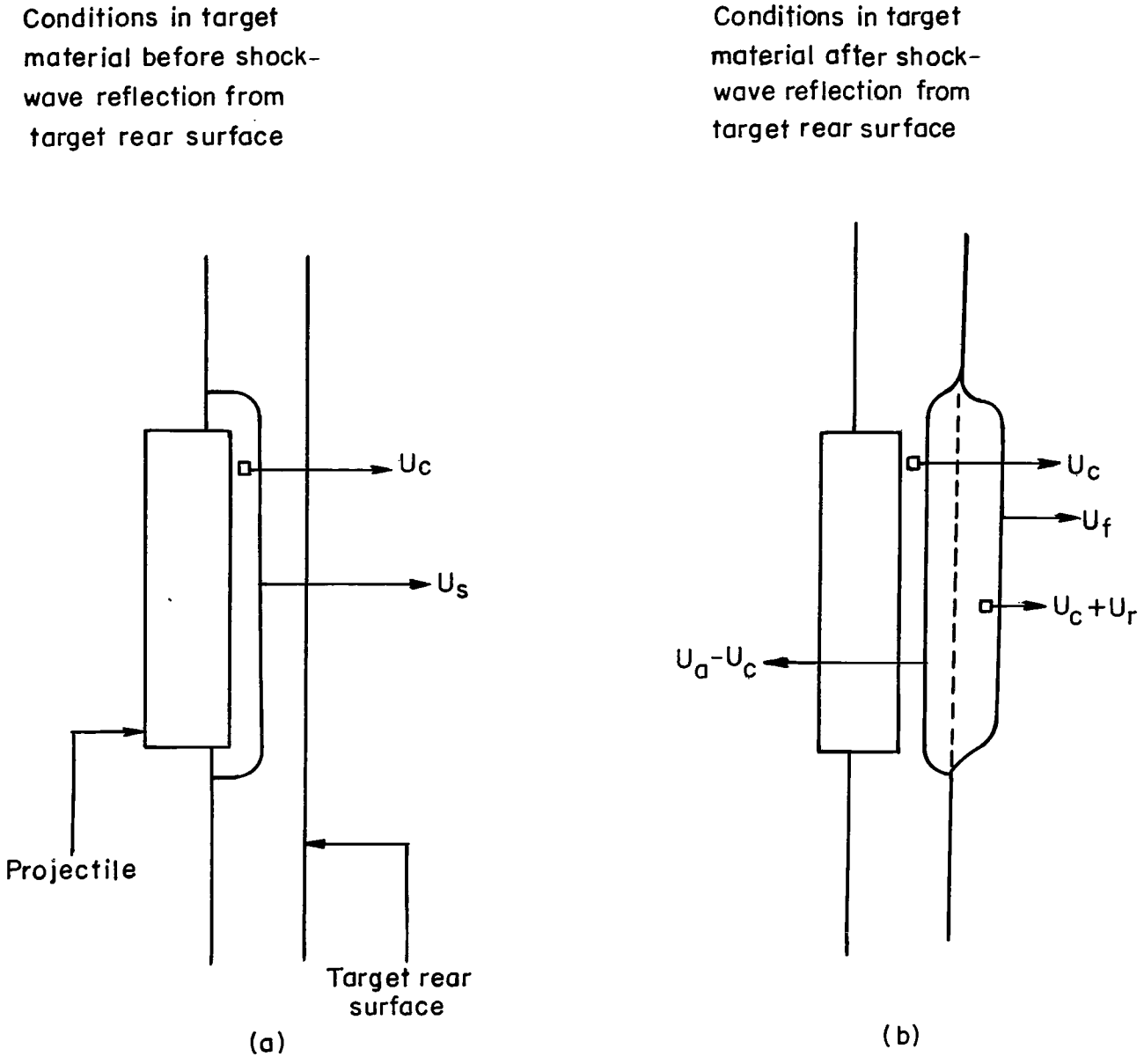

Figure 4.- Conditions produced in target with impact of projectile.

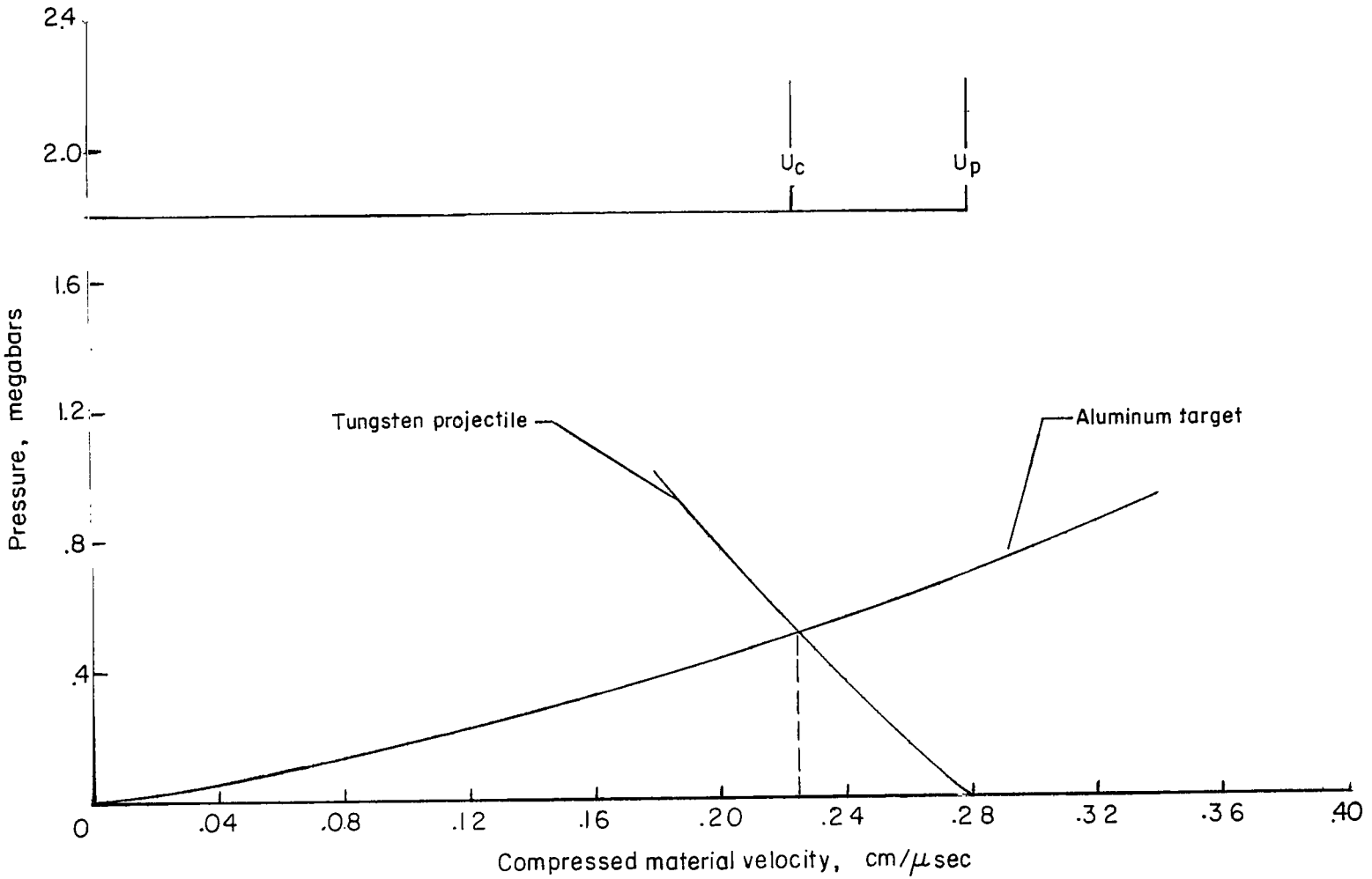

Figure 5.- Graphical solution to determine projectile impact velocity.

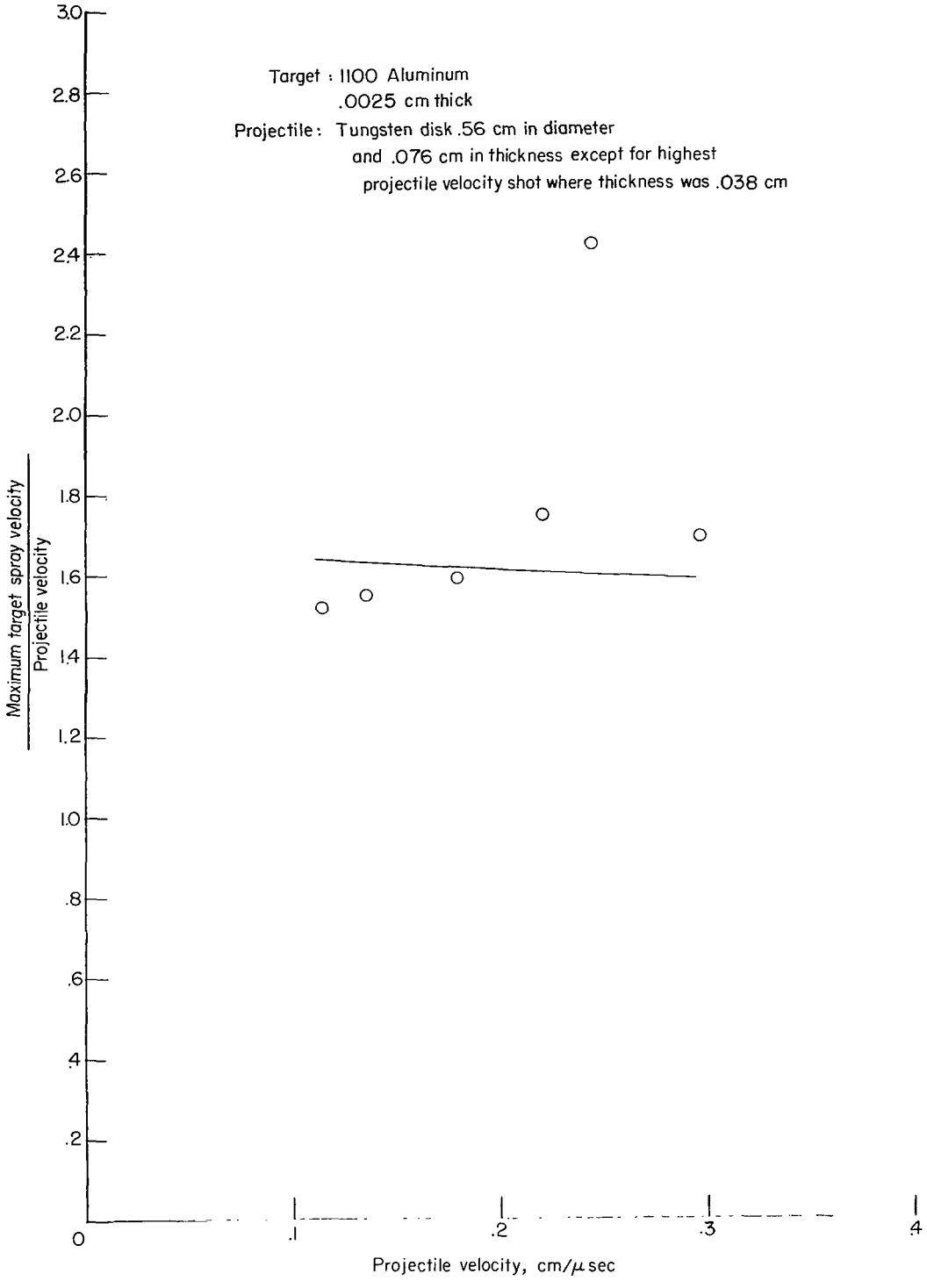

Figure 6.- Comparison of experimental and predicted ratio of maximum target-material spray velocity and projectile velocity with a 1100 aluminum target 0.0025 cm thick.

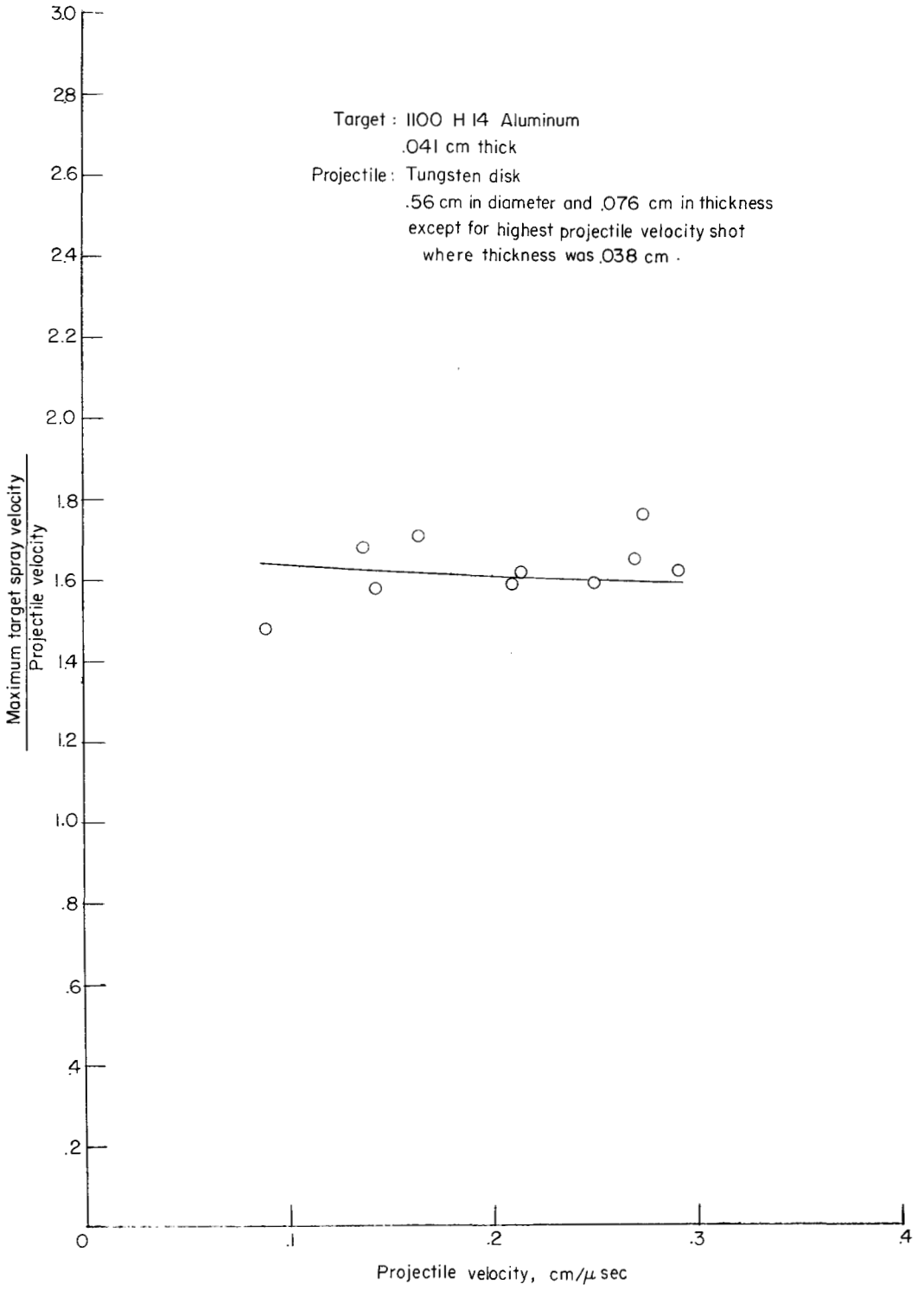

Figure 7.- Comparison of experimental and predicted ratio of maximum target-material spray velocity and projectile velocity with a 1100 H14 aluminum target 0.041 cm thick.

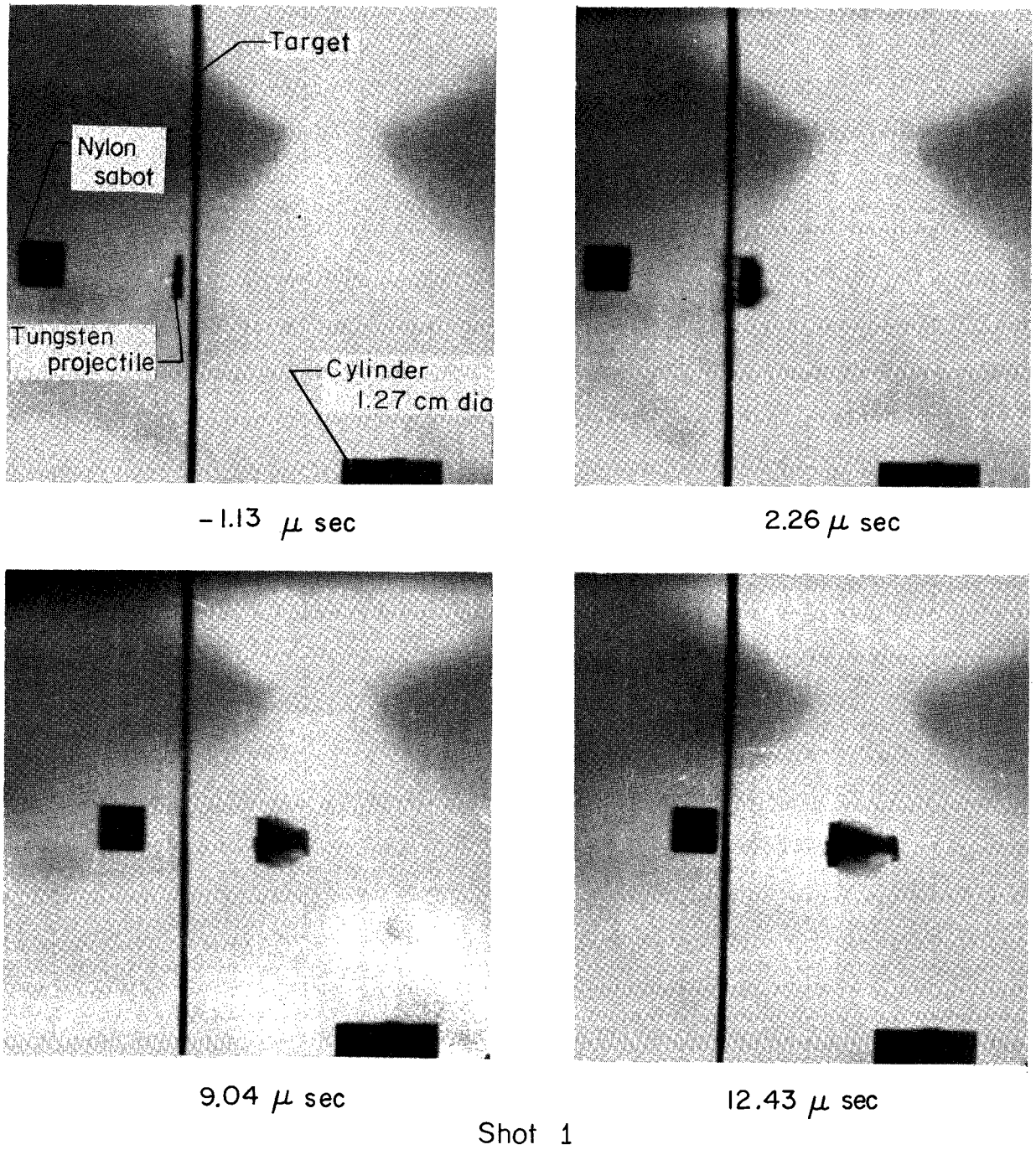

L-66-4419

Figure 8.- A tungsten disk 0.56 cm in diameter and 0.076 cm thick impacting a 1100 aluminum target 0.0025 cm thick at 0.113 cm/μsec. $U_f/U_p = 1.52$.

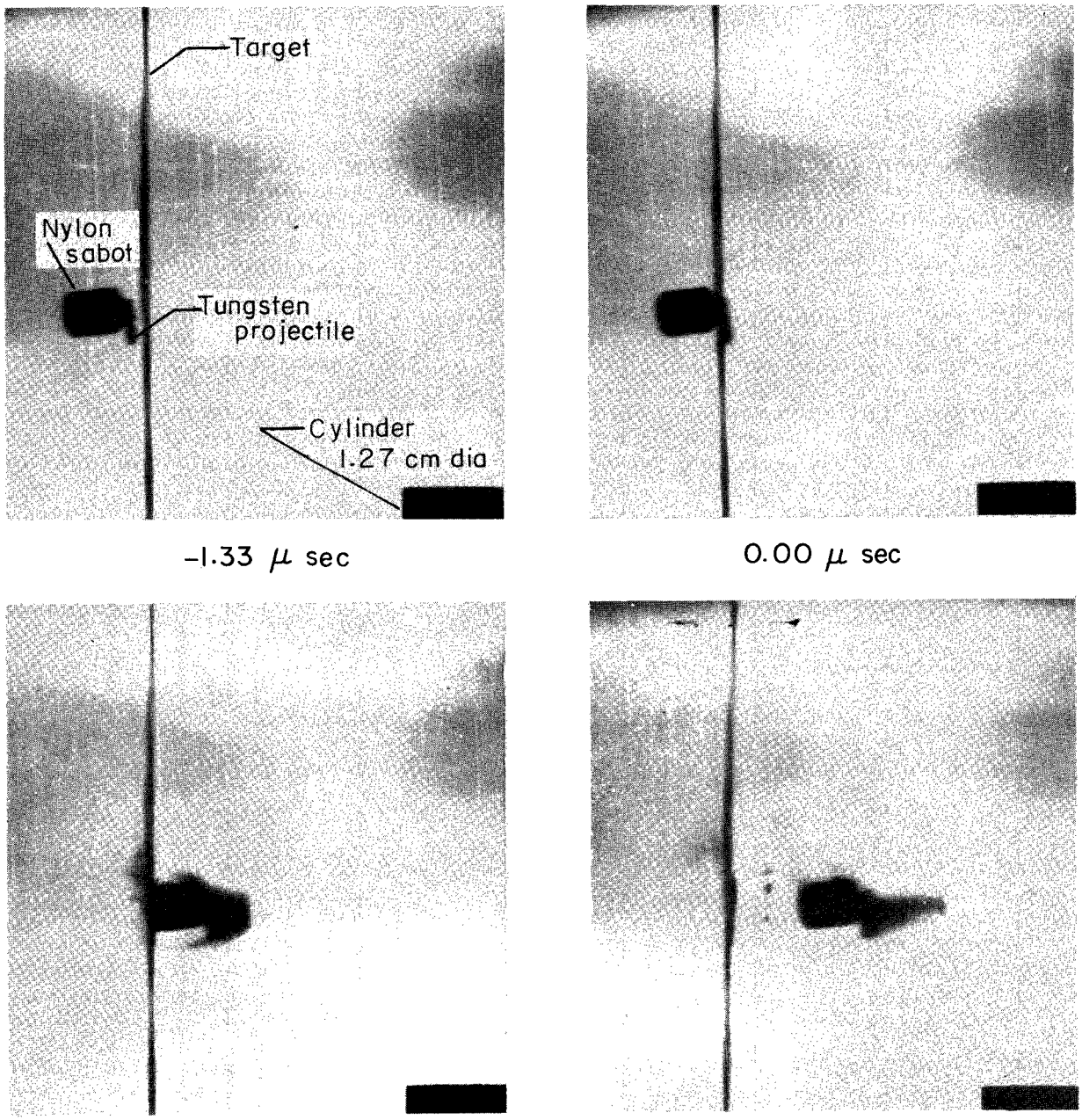

L-66-4420

Figure 9.- A tungsten disk 0.56 cm in diameter and 0.076 cm thick impacting a 1100 aluminum target 0.0025 cm thick at 0.179 cm/μsec. $U_f/U_p = 1.59$.

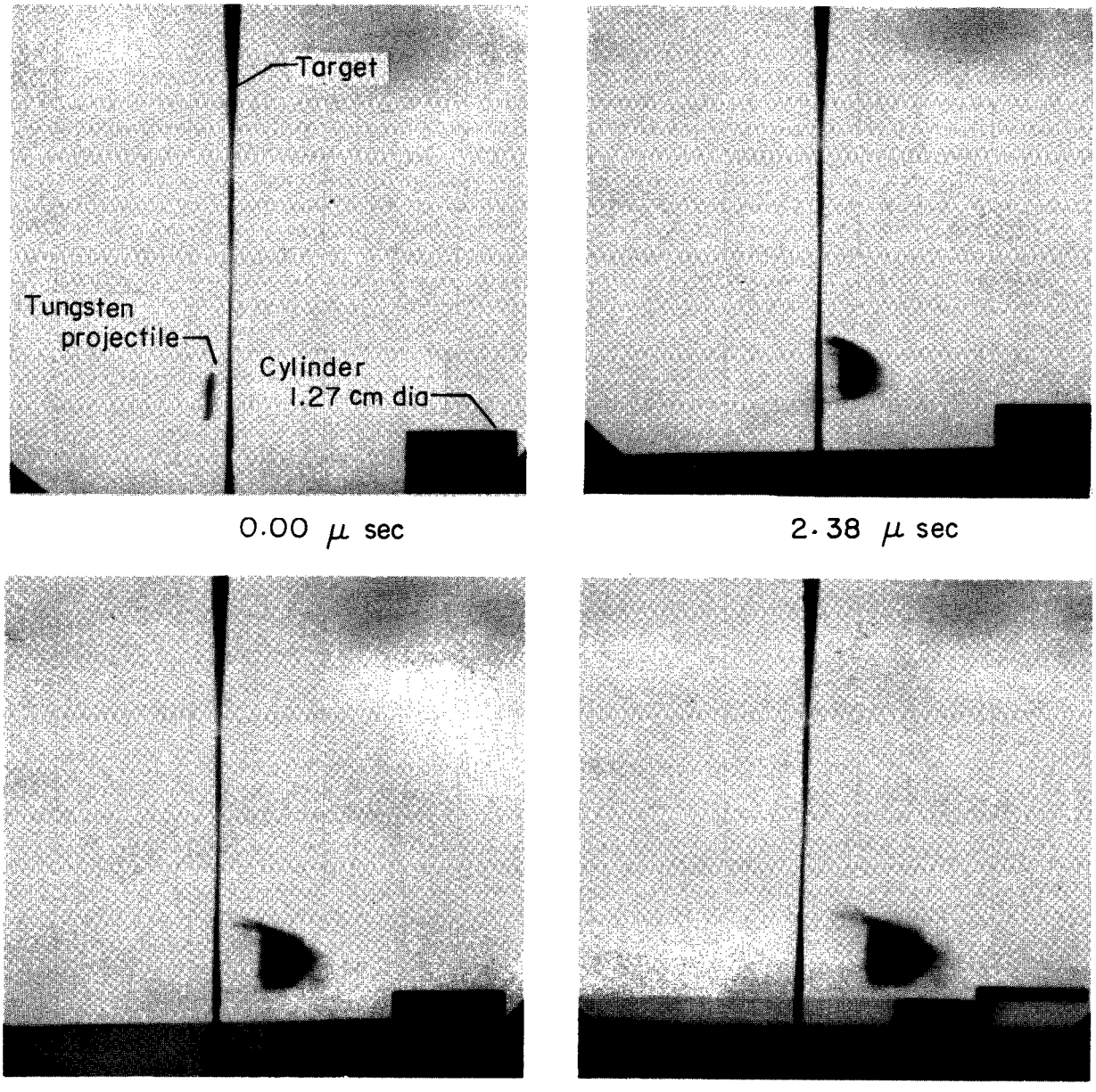

L-66-4421

Figure 10.- A tungsten disk 0.56 cm in diameter and 0.076 cm thick impacting a 1100 aluminum target 0.0025 cm thick at 0.219 cm/μsec. $U_f/U_p = 1.74$.

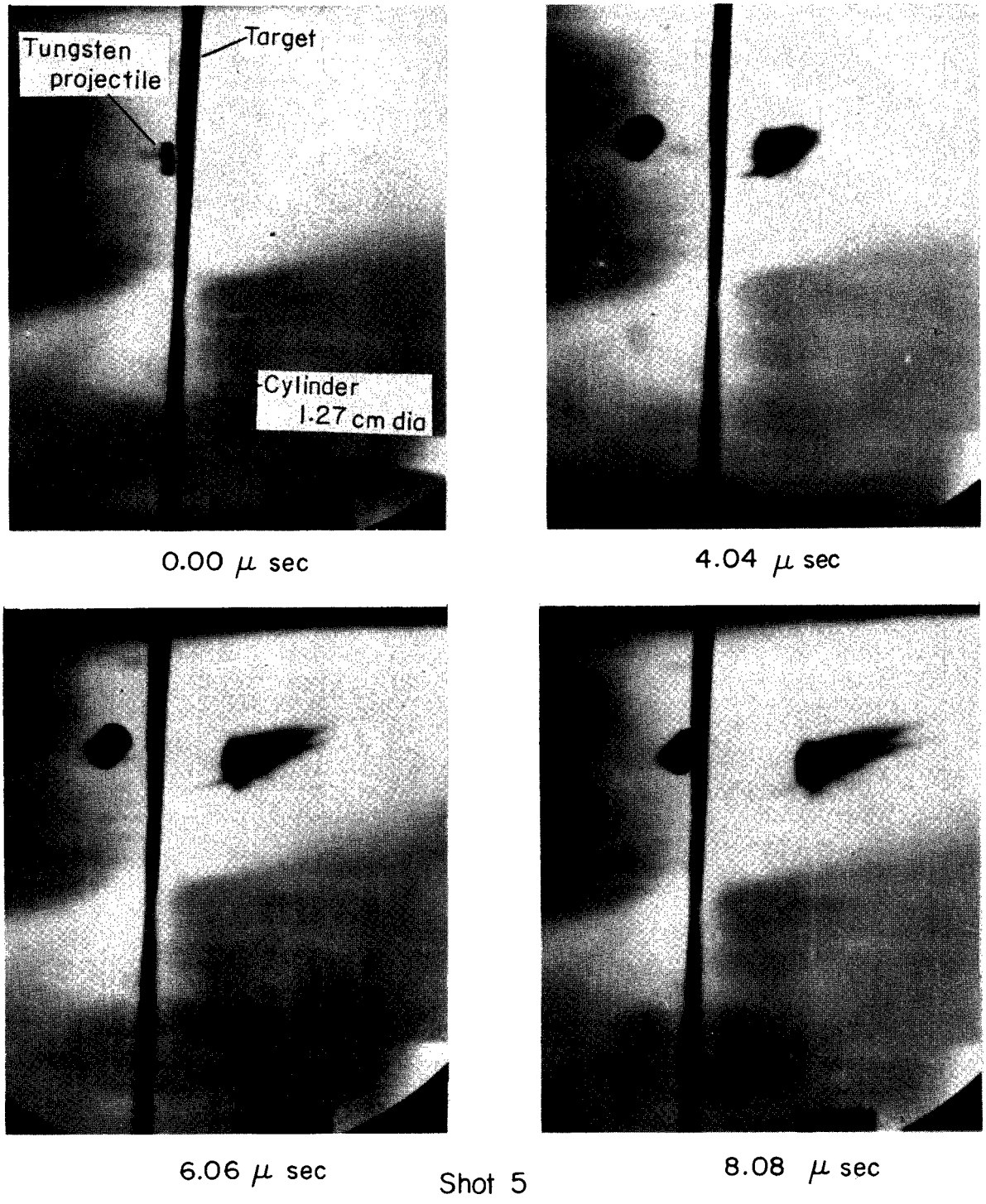

L-66-4422

Figure 11.- A tungsten disk 0.56 cm in diameter and 0.076 cm thick impacting a 1100 aluminum target 0.0025 cm thick at 0.243 cm/μsec. $U_f/U_p = 2.42$.

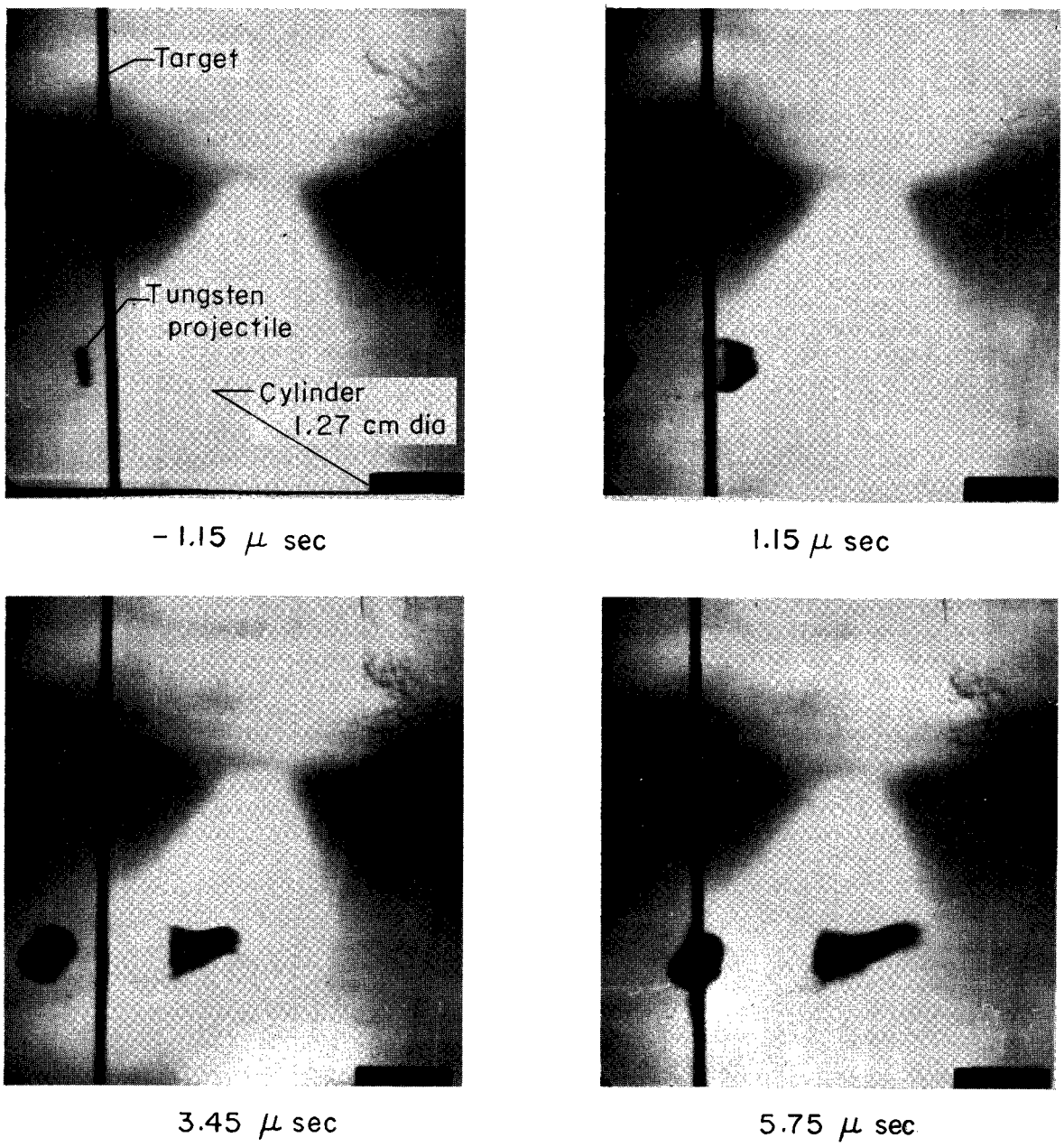

L-66-4423

Figure 12.- A tungsten disk 0.56 cm in diameter and 0.038 cm thick impacting a 1100 aluminum target 0.0025 cm thick at 0.295 cm/μsec. $U_f/U_p = 1.69$.

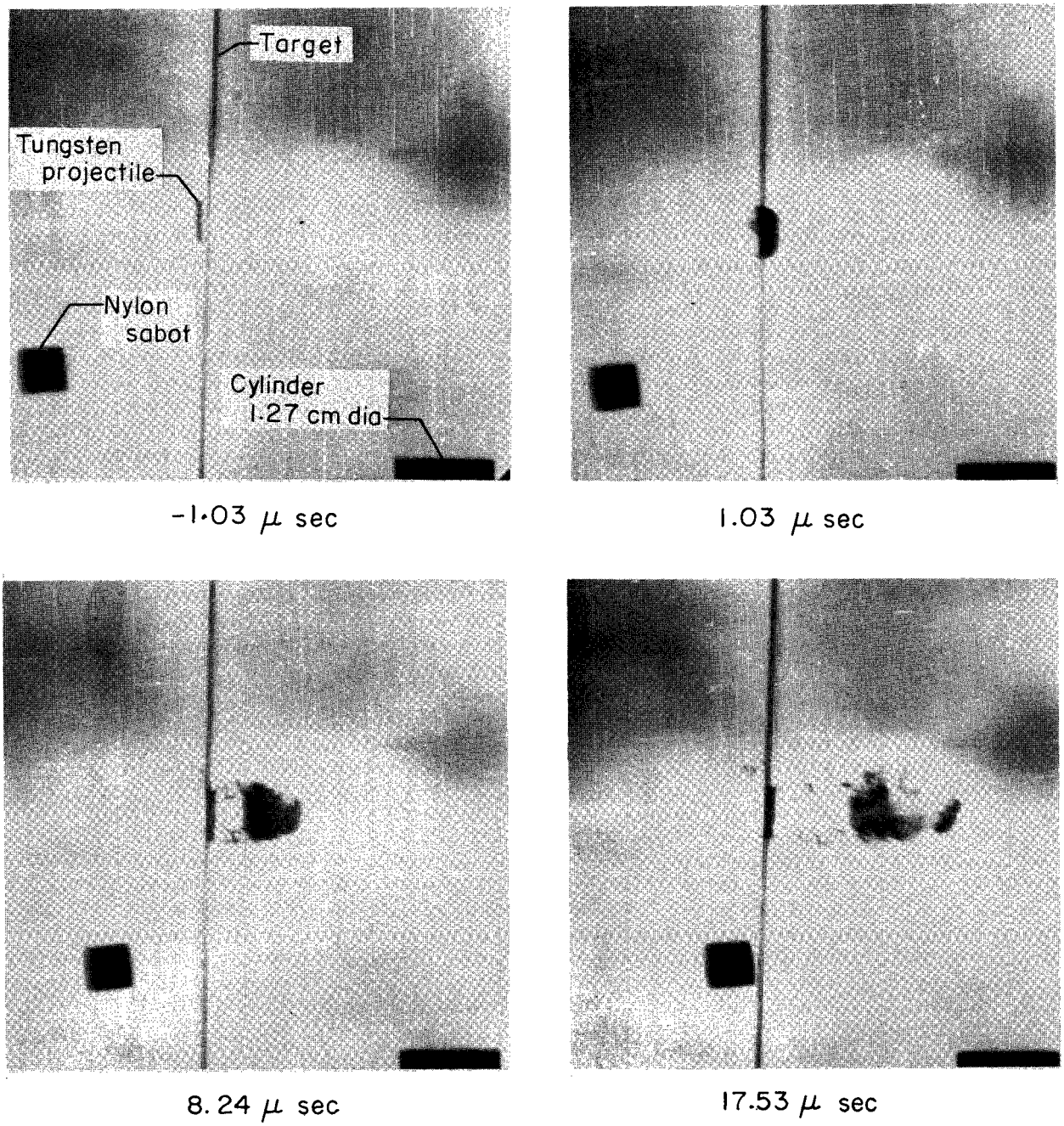

L-66-4424

Figure 13.- A tungsten disk 0.56 cm in diameter and 0.076 cm thick impacting a 1100 H14 aluminum target 0.041 cm thick at 0.089 cm/μsec. $U_f/U_p = 1.48$.

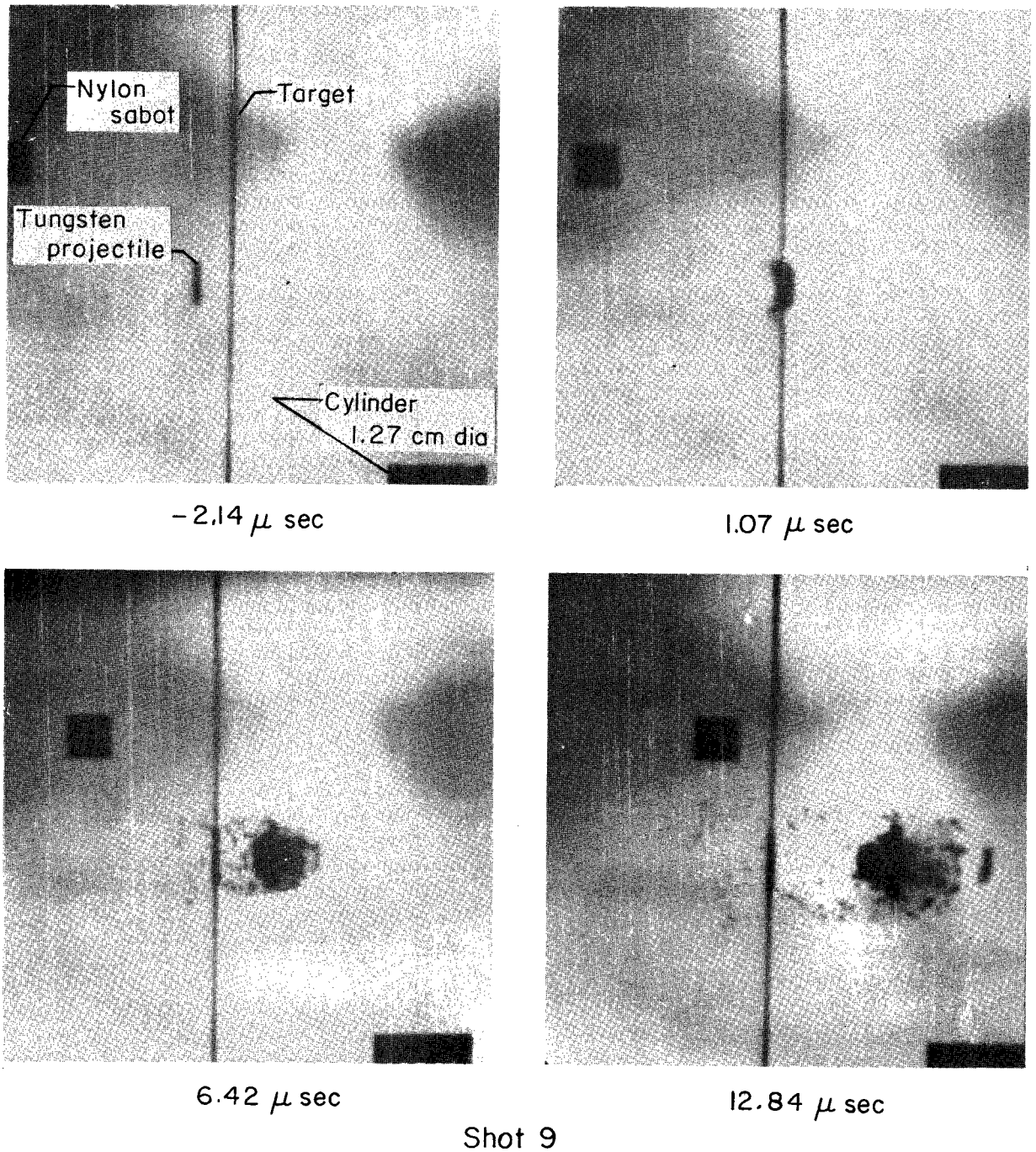

L-66-4425

Figure 14.- A tungsten disk 0.56 cm in diameter and 0.076 cm thick impacting a 1100 H14 aluminum target 0.041 cm thick at 0.143 cm/μsec. $U_f/U_p = 1.58$.

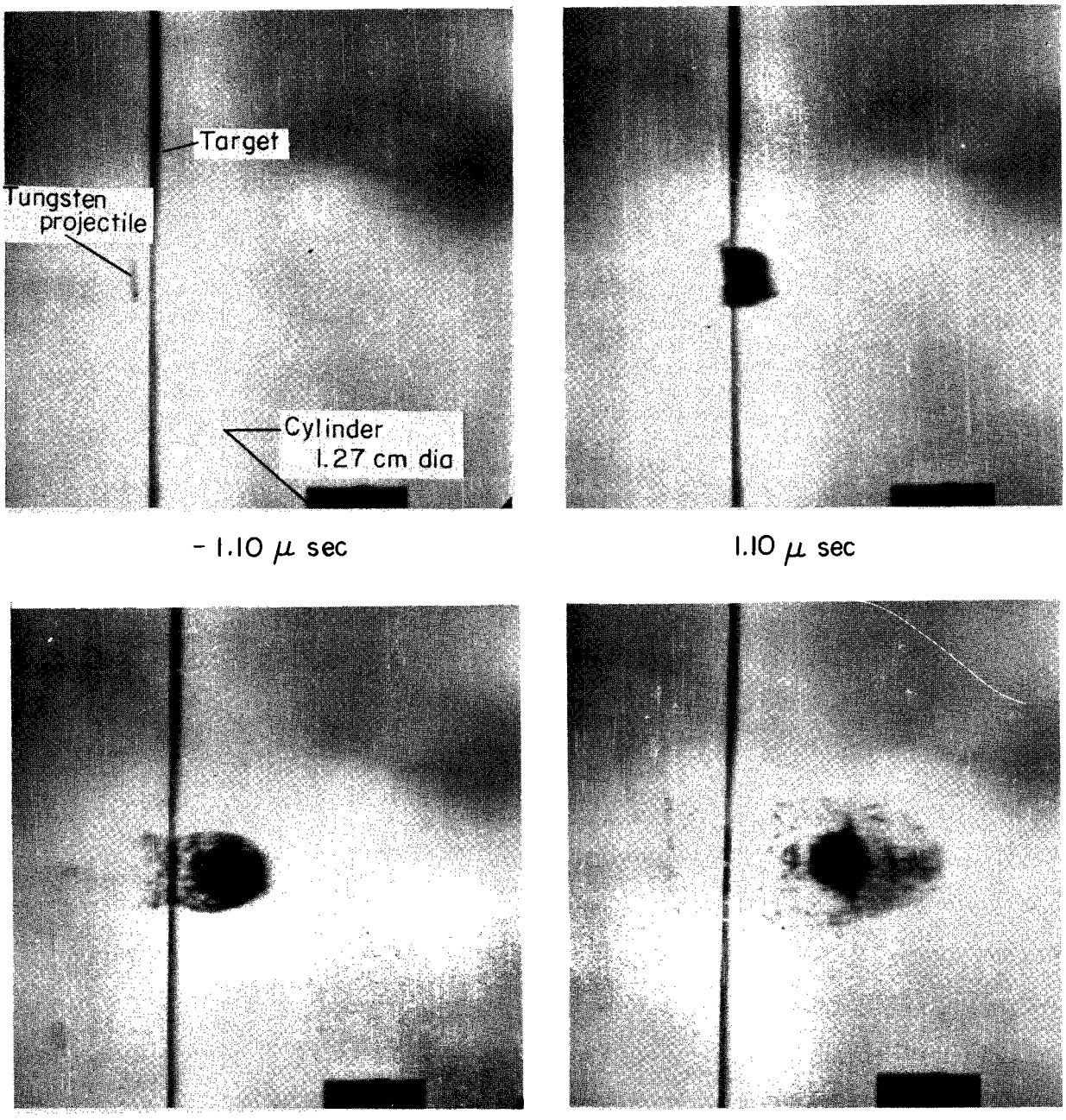

L-66-4426

Figure 15.- A tungsten disk 0.56 cm in diameter and 0.076 cm thick impacting a 1100 H14 aluminum target 0.041 cm thick at 0.209 cm/μsec. $U_f/U_p = 1.59$.

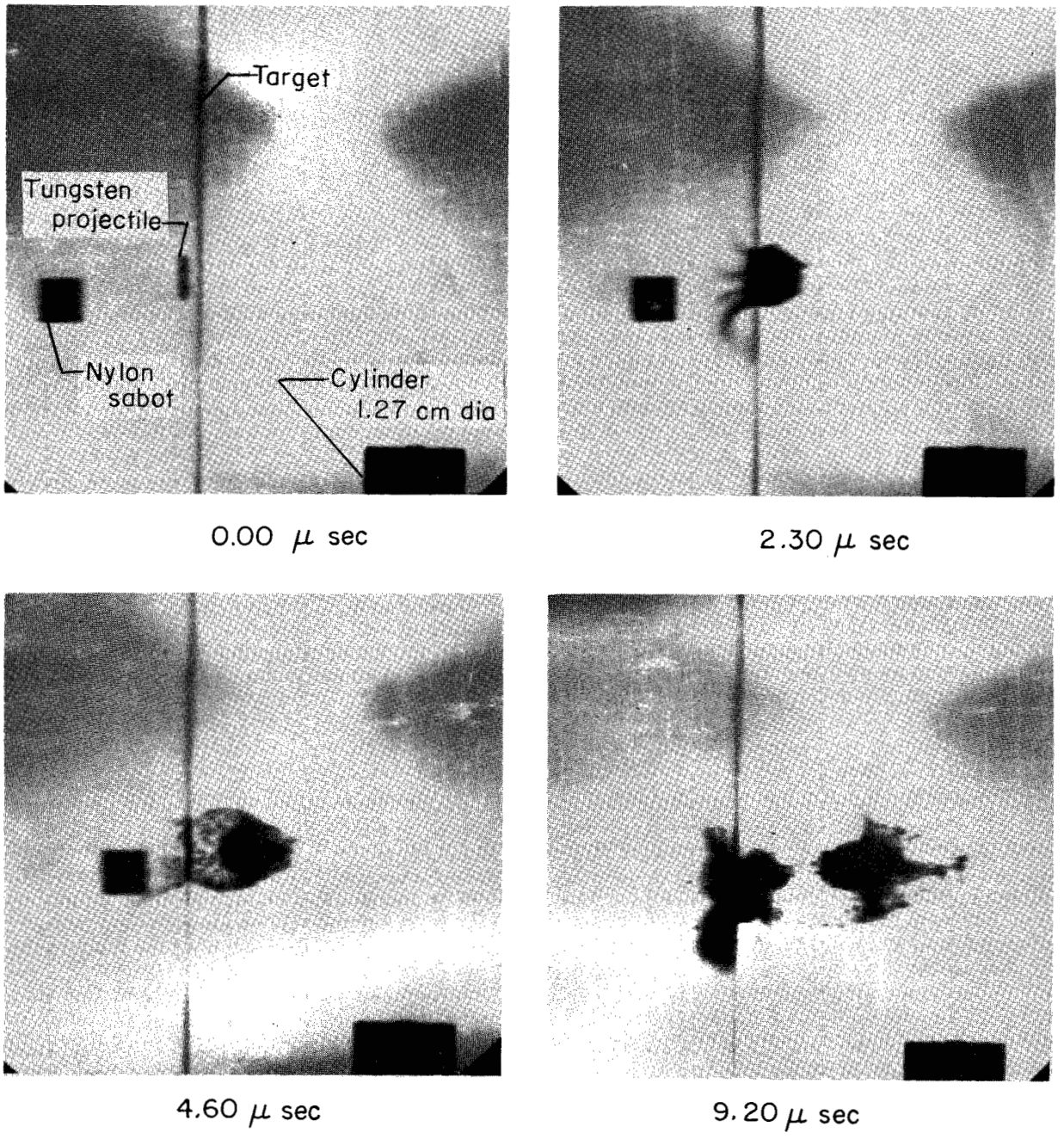

L-66-4427

Figure 16.- A tungsten disk 0.56 cm in diameter and 0.076 cm thick impacting a 1100 H14 aluminum target 0.041 cm thick at 0.212 cm/μsec. $U_f/U_p = 1.62$.

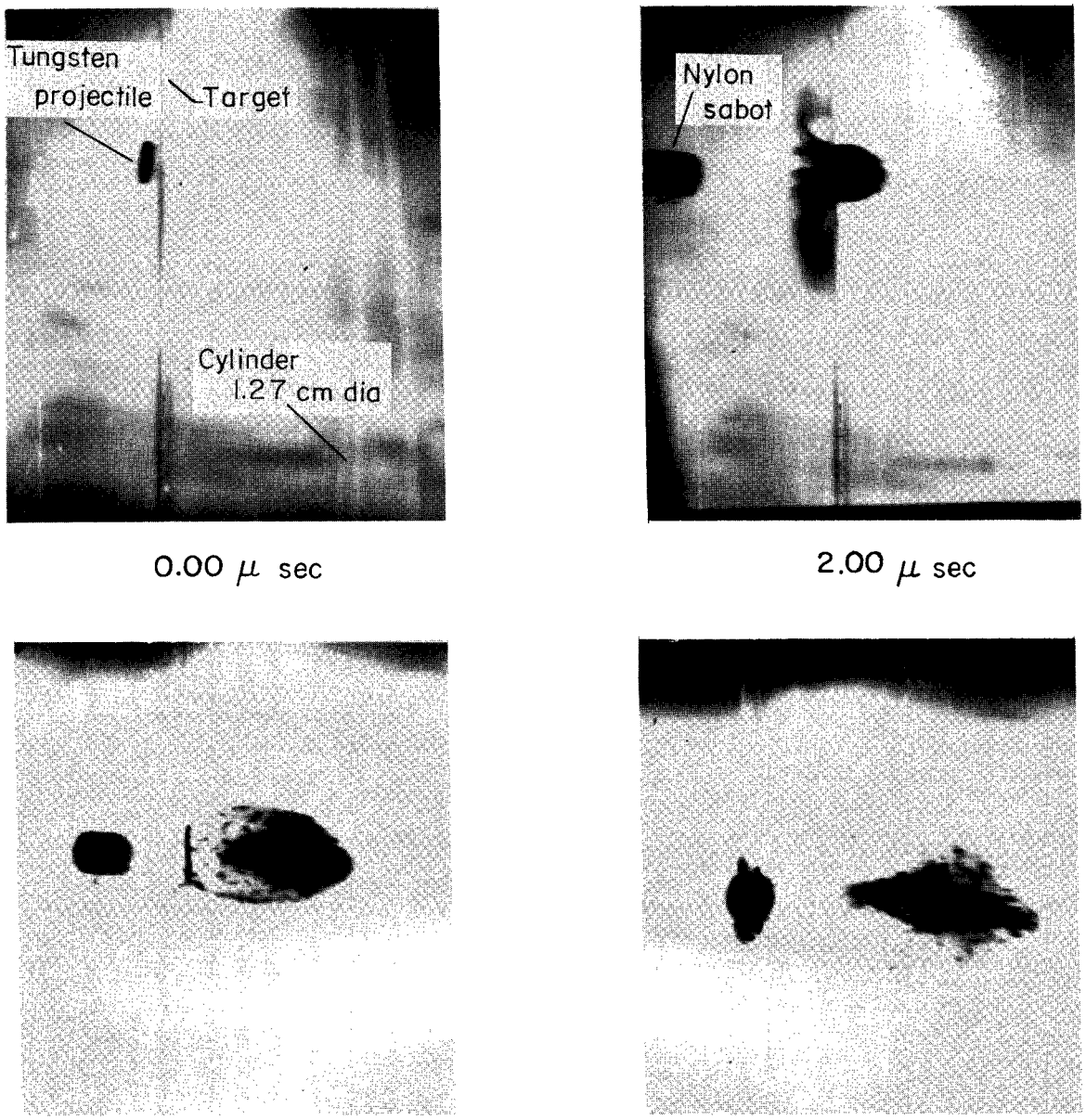

L-66-4428

Figure 17.- A tungsten disk 0.56 cm in diameter and 0.076 cm thick impacting a 1100 H14 aluminum target 0.041 cm thick at 0.250 cm/μsec. $U_f/U_p = 1.59$.

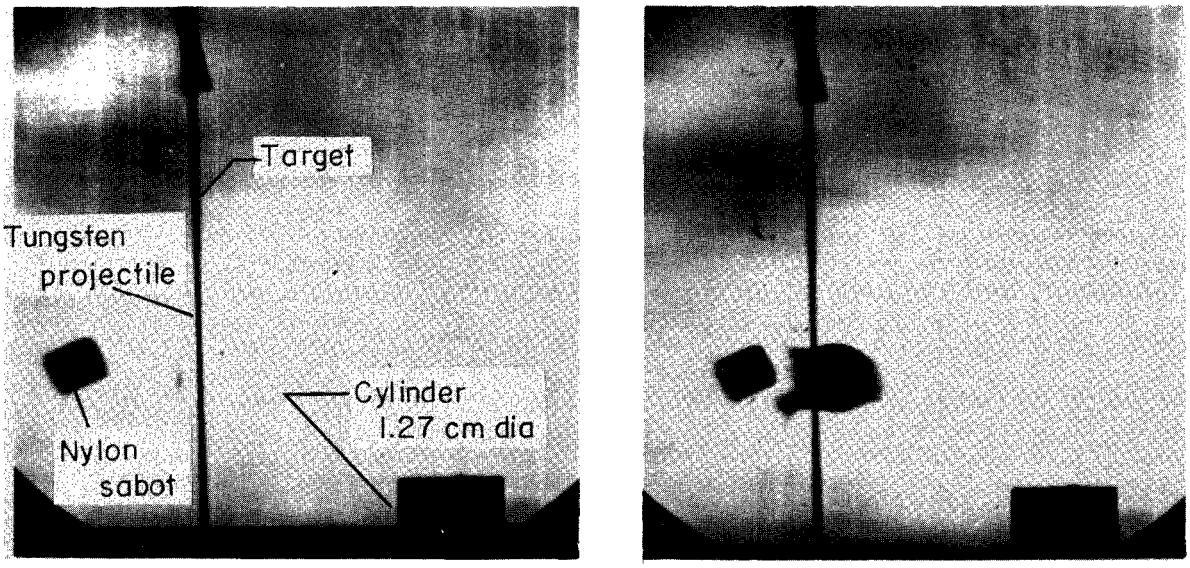

L-66-4429

Figure 18.- A tungsten disk 0.56 cm in diameter and 0.038 cm thick impacting a 1100 H14 aluminum target 0.041 cm thick at 0.291 cm/μsec. $U_f/U_p = 1.62$.

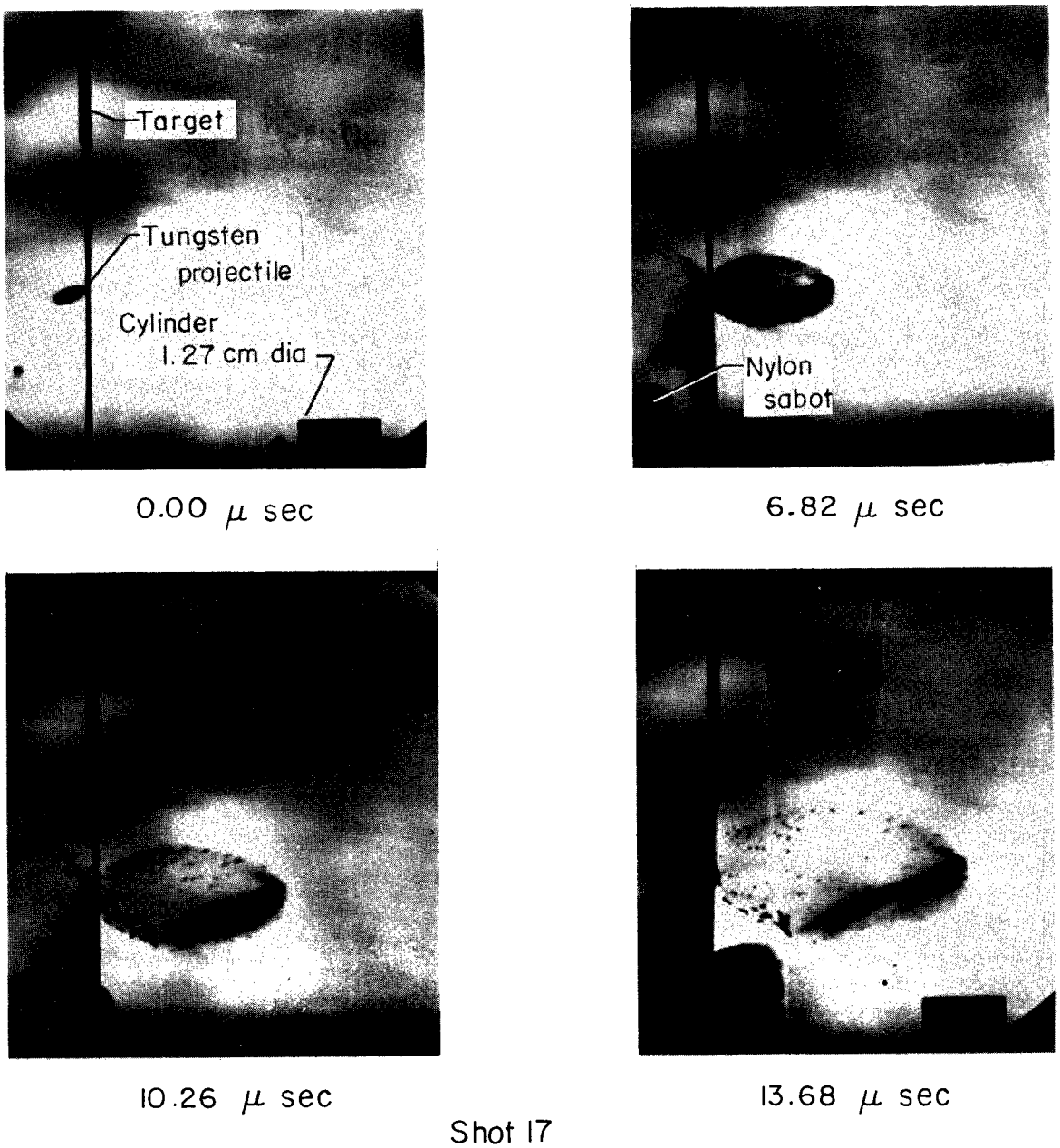

L-66-4430

Figure 19.- A tungsten disk 0.56 cm in diameter and 0.038 cm thick impacting a 1100 H14 aluminum target 0.041 cm thick at 0.294 cm/μsec. $U_f/U_p = 1.00$.

"The aeronautical and space activities of the United States shall be conducted so as to contribute . . . to the expansion of human knowledge of phenomena in the atmosphere and space. The Administration shall provide for the widest practicable and appropriate dissemination of information concerning its activities and the results thereof."

—NATIONAL AERONAUTICS AND SPACE ACT OF 1958

NASA SCIENTIFIC AND TECHNICAL PUBLICATIONS

TECHNICAL REPORTS: Scientific and technical information considered important, complete, and a lasting contribution to existing knowledge.

TECHNICAL NOTES: Information less broad in scope but nevertheless of importance as a contribution to existing knowledge.

TECHNICAL MEMORANDUMS: Information receiving limited distribution because of preliminary data, security classification, or other reasons.

CONTRACTOR REPORTS: Technical information generated in connection with a NASA contract or grant and released under NASA auspices.

TECHNICAL TRANSLATIONS: Information published in a foreign language considered to merit NASA distribution in English.

TECHNICAL REPRINTS: Information derived from NASA activities and initially published in the form of journal articles.

SPECIAL PUBLICATIONS: Information derived from or of value to NASA activities but not necessarily reporting the results of individual NASA-programmed scientific efforts. Publications include conference proceedings, monographs, data compilations, handbooks, sourcebooks, and special bibliographies.

Details on the availability of these publications may be obtained from:

SCIENTIFIC AND TECHNICAL INFORMATION DIVISION

NATIONAL AERONAUTICS AND SPACE ADMINISTRATION

Washington, D.C. 20546